Supporting Information

Stagnation region of μMM

After each aqueous solution of CTAB and NaSal were injected at the lateral arms of the T-shaped microchannel, the μMM was formed in the main channel (see Figure S1 and SI-Movie-1). Figure S1 highlights the "tip" region in the μMM exhibiting a trapezoidal-like shape due to the flow field created by the corners of the T-shaped microchannel.

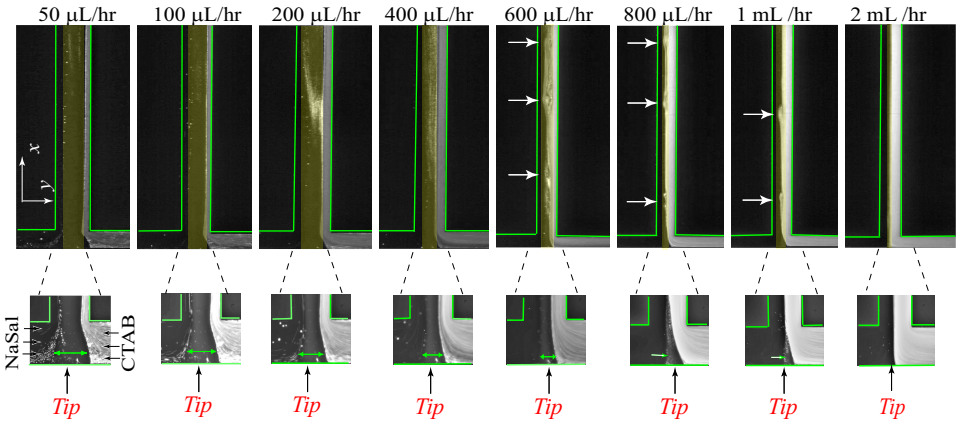

Figure 1: The μMM is anchored at the stagnation "tip" region. The μMM can move along y-direction but is immbolized in the x-direction (evidenced by SI-Movie-1) . The thickness of the "tip" region decreased with increasing flow rates, allowing the μMM to move at flow rates $Q > 600$ μL/hr. The white arrows highlight the formation of wave and vortex-like patterns (see more details in SI-Movie-2). The channel width is 300 μm.

We suggest that the corner of the T-shaped channel stretch the μMM and induce a trapezoidal zone in the stagnation region of the μMM. Further experiments will be performed with different channel geometries without the presence of the stagnation region in the μMM in our future work. The thickness and shape of the μMM's "tip" region decreased as the flow rate increased (see Figure S1), suggesting that the μMM begins to detach from the stagnation region.

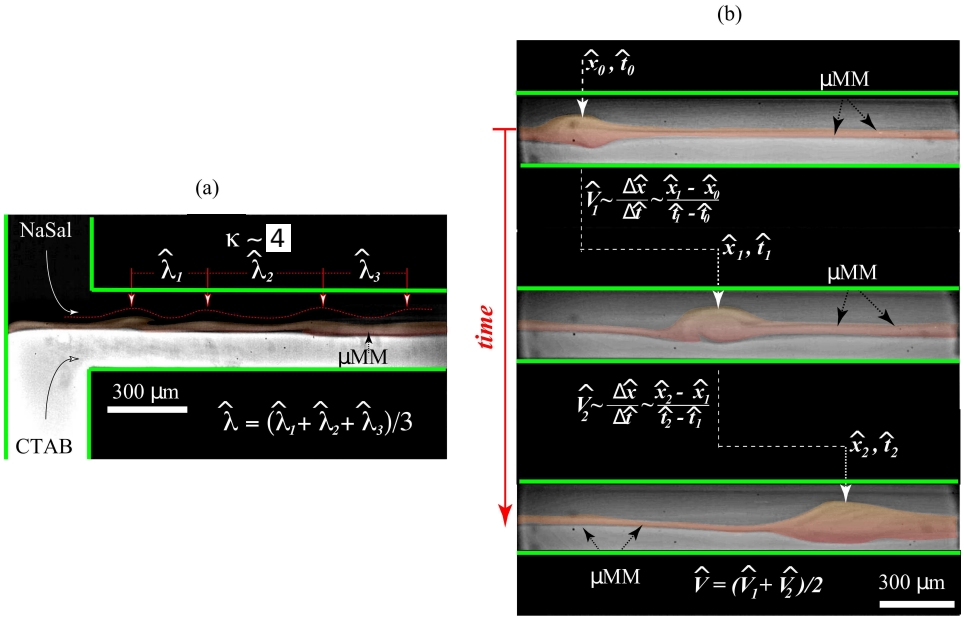

Figure 2: Representative example of the unstable uMM flowing at 800 μL/hr. (a) Representative dimensional wave number $\hat{k}$ and wavelength $\hat{\lambda}$ of an unstable μMM. (b) The propagation speed $\hat{V}$ of an unstable μMM.

Estimating material parameters of the μMM

We measured the μMM's thickness and calculated the dimensionless wave number k, wavelength λ, and ν by analyzing μ–PIV and fluorescence microscopy and using Eq (4)–Eq (7) in the main manuscript. More specifically, we first measured the dimensional wavelength $\hat{\lambda}$ and the propagation speed $\hat{V}$ of the μMM at which it travels along the T-shaped microchannel, see definitions in Figure S2 by processing the images and videos of the μMM for each flow rate. $\hat{\lambda}$ was measured and averaged from more than 30 images, with the averaged dimenional $\hat{\lambda}$ shown as open square symbols in Figure 5(b) in the main manuscript. Equivalently, the instability is expected to develop at a distance $L \sim \hat{V} \times \Delta t$ from the stagnation region. The distance and time of the instability was measured and averaged from consecutive frames, with the experimental value of the dimensional propagation speed $\hat{V}$ being plotted in Figure 5(c) in the main manuscript.

Once we obtained these experimental values of the μMM, we approx-

imated the values of k (dimensionless wavenumber) and σ (dimensionless growth rate) as follows: each flow rate has a fixed value of pressure gradient P, for this fixed P we obtained the maximum value of σ in Equation 2 in the manin manuscript over all positive values of k using standard routines in Matlab. The k that gives rise to the maximum is the dimensionless wavenumber of the most unstable mode in the μMM. Using the values of k obtained in the previous step, we computed the dimensionless growth rate σ using Equation 2 in the main manuscript and dimensionless speed v of the disturbance in Equation 7 in the main manuscript. Lastly we obtained the values of the growth rate $\hat{\sigma}$ by using Equation 3 in the main manuscript.

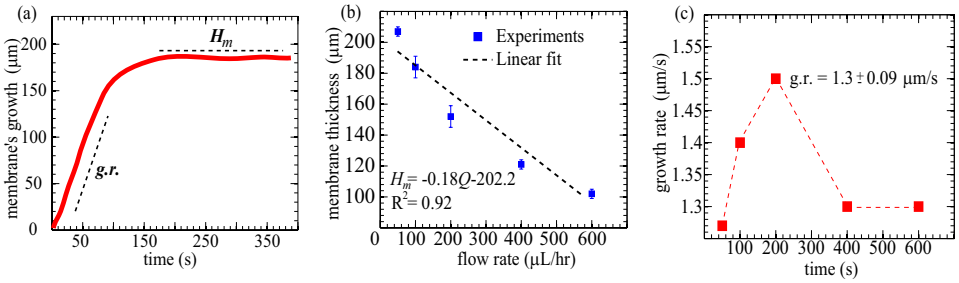

Figure 3: (a) Schematics of the temporal evolution of the μMM growth. (b) Averaged μMM thickness approximated by using the value in the plateau region shown in (a). The black dashed line shows the linear fit of the experimental values. (c) Rate of growth (g.r.) of the μMM approximated by using the slope of the black dashed line in (a) before reaching the plateau region.

Figure S3 shows the temporal evolution of the μMM's growth. For Q ranging between 50–600 μL/hr (Re ~0.07–0.58), H_m reached a plateau region after ~130 s (see Figure 3(c) in the main manuscript), indicating that H_m is independent of the position along x-axis once the μMM is completely equilibrated. Figure S3(a) presents the schematic of the growth behavior of the μMM. Figure S3(b) shows the monotonic decrease of H_m with increasing flow rate Q. By performing a linear fit of the H_m of the stable μMM (see horizontal dash-black line in Figure S3(a)), we approximated μMM thickness H_m for those Q–values where the μMM was unstable. We also obtained the value of the slope (dashed black line in Figure S3(a)) for each flow rate to estimate the growth rate ($g.r$) of the μMM (see Figure S3(c)). We noticed that the rate of growth ($g.r$~1.3±0.09 μm/s) of the μMM remained on the same order of magnitude for the range of Q where μMM was stable, sug-

gesting that the diffusion-reaction kinetics between the CTAB and NaSal is independent of the flow rate used to form stable μMM. This simple method could be extrapolated to perform real time studies of the structural evolution of anionic, non-ionic and zwitterionic micelles into μMM or different thermodynamic phases (e.g., liquid crystals or lipid bilayers).